CHAPTER 5

Effect of Doped Spiro-OMeTAD Based HTL on the Performance of FTO/ZnO Nanorods/$CH_3NH_3PbI_3$/Spiro-OMeTAD/Pd Perovskite Solar Cells*

Contents

*Part of this work has been published as:

1. Jarwal, Deepak Kumar, et al. "Fabrication and TCAD validation of ambient air-processed ZNRs/$CH_3NH_3PbI_3$/Spiro-OMeTAD solar cells." *Superlattices and Microstructures* (2020).

CHAPTER 5

Effect of Doped Spiro-OMeTAD Based HTL on the Performance of FTO/ZnO Nanorods/$CH_3NH_3PbI_3$/Spiro-OMeTAD/Pd Perovskite Solar Cells

5.1 Introduction

We have investigated the performance characteristics of FTO/ZnO Seed Layer/ZnO Nanorods/$CH_3NH_3PbI_3$/PTAA/Au where ZnO nanorods (ZNRs) have been synthesized from the four different types seed layers by hydrothermal method in Chapter-4. The ZNRs have increased mobility, easy synthesis, low-temperature processing, and high stability [115], [126], [165]. Although ZNRs based PSCs have good power conversion efficiency (PCE), some modification is required in the synthesis process of ZNRs to remove voids and traps on the surface. Son et al. [90] have reported the maximum PCE of 14.35% using $(NH_4)_2TiF_6$ treated ZNRs based ETL in the PSCs. The surface-treated ZNRs minimize the recombination for the generated charge carriers. On the other hand, the use of doping engineered hole transport layer (HTL) in the PSCs improves their efficiency, stability, and environment-friendly operations [127], [166]-[168]. It is found that the mobility/conductivity of spiro-OMeTAD can be increased by appropriate doping. The common p-type dopants to the spiro-OMeTAD are bis(trifluoromethane) sulfonamide lithium salt (Li-TFSI) and 4-tert-butylpyridine (TBP) [166]. It is observed that lithium salt helps in the oxidation process of spiro-OMeTAD, whereas TBP improves the conductivity of the active layer by dissolving in the perovskite layer [169]. In this chapter, we will investigate the effects of doped HTL based ZNRs/$CH_3NH_3PbI_3$/Spiro-OMeTAD based hybrid PSCs using LiTFSI and TBP

dopants. The experimental results have been compared with the commercially available SetFos^{TM} TCAD simulation data for their validation. The outline for the rest of this chapter is as follow:

Section 5.2 describes the details of the synthesis process of ZNRs and the fabrication steps of PSCs. The simulation methodology and the factors affecting the parameters of simulated solar cells are discussed in Section 5.3. The measurement results, their comparison with simulated results, and discussion are presented in Section 5.4. Finally, Section 4.5 summarizes the finding and observations of this chapter.

5.2 Experimental Details

5.2.1 Thin Film Growth and Perovskite Solar Cells Fabrication

FTO coated glass substrate in 15 mm × 15 mm square size was cleaned ultrasonically step by step in a soap solution, acetone, and isopropanol, respectively, for 15 minutes each [170]. The wet cleaned substrates were kept in the plasma chamber for 10 minutes for dry cleaning under nitrogen and argon flow to make the surface more hydrophilic. Two types of PSCs with fixed ZnO NRs ETL and variation in HTL (undoped and spiro-OMeTAD) were fabricated on FTO coated glass substrates. First of all, the ZnO QDs solution was prepared using dissolving zinc acetate dihydrate in 2-methoxy ethanol at 60^0 C and stirred for 24 hours under an inert environment (Nitrogen gas) [171]. Further, the solution was filtered using a 0.22 um PVDF membrane to remove uncreated particles. A very thin seed layer of as-synthesized ZnO quantum dot was deposited using a spin coating on cleaned FTO substrate to make uniformly distributed ZnO nanorods. The ZnO NRs were grown on ZnO QDs coated FTO substrate using a solvothermal process [154]. In brief, the precursor solution was

prepared by mixing of 500 mM zinc acetate and 500 mM HTMA in de-ionized (DI) water. The mixed precursor solution was then transferred in Teflon lined cylindrical autoclave. The ZnO coated FTO substrates were kept in an autoclave with an angle. The autoclave was moved in a digital muffle furnace at a constant temperature of 95^0 C for 4 hours to obtain ZnO NRs with an average length of 400 nm. After the growth of ZnO NRs, the samples were rinsed in DI water for removal of unreacted salts and annealed at 250^0 C for 1 hour to make a fully crystalline phase. Further, surface modification using $TiCl_4$ treatment was performed by dipping in 40 mM $TiCl_4$ solution in DI water for 30 minutes at 70^0 C [116]. The $TiCl_4$ treatment overcomes the separation between two consecutive ZnO NRs. The perovskite was deposited on grown ZnO NRs using two-step spin coating methods. The precursor solution was prepared by dissolving 462 mg lead iodide (PbI_2) and 10 mg methylammonium iodide (CH_3NH_3I) in 1 ml DMF and 1 ml isopropanol, respectively. Both the inorganic material (PbI_2) and organic material (CH_3NH_3I) were deposited on grown ZnO NRs sample using spin coater (SPM-150LC, GmbH). The precursor's solutions of PbI_2 and CH_3NH_3I were deposited at 2000 and 3000 rpm, respectively, for 30 seconds. The overall thickness of 300 nm was achieved for the perovskite film. The obtained perovskite layer (active layer) was annealed at 90°C for 30 minutes to evaporate the solvent. Further, HTL of undoped spiro-OMeTAD and doped spiro-OMeTAD (dopant are LiTFSI and TBP) were deposited separately for the identical thickness of 80 nm [172]. Finally, 100 nm Pd was deposited using a thermal evaporation coating unit (Hind High Vac, model smart coat 3.0A) at a vacuum of 2×10^{-6} mbar. The fabrication steps for the proposed PSCs have been illustrated in Figure 5.1 (a). The complete device structure (FTO/ ZNRs/Perovskite/Spiro-OMeTAD/Pd) of the fabricated PSCs is shown in Figure 5.1(b).

5.2.2 Film and Device Characterization

The surface roughness is measured by atomic force microscopy (AFM, model: NaioAFM from Nanosurf, Switzerland) in dynamic mode. The surface morphology was taken by high resolution scanning electron microscope-HRSEM (Nova Nano SEM 450, FEI, USA). The absorbance spectra were obtained using UV-VIS spectroscopy (Jesco Corp.). The current density-voltage characteristic was obtained using a parameter analyzer (KeySight, B1500A). The light of one sun (100 mW/cm^2) was obtained from a solar simulator (Model: SS50AAA, AM 1.5G Photo Emission Tech Inc, USA). The external quantum efficiency (EQE) of the PSC was measured using a digital multimeter (Agilent, 34410A) and a monochromator (Princeton Instruments, SP2150i). The optical power density of the light sources (Halogen lamp, 150 watts) was measured using a PM100D (from Thorlabs) detector.

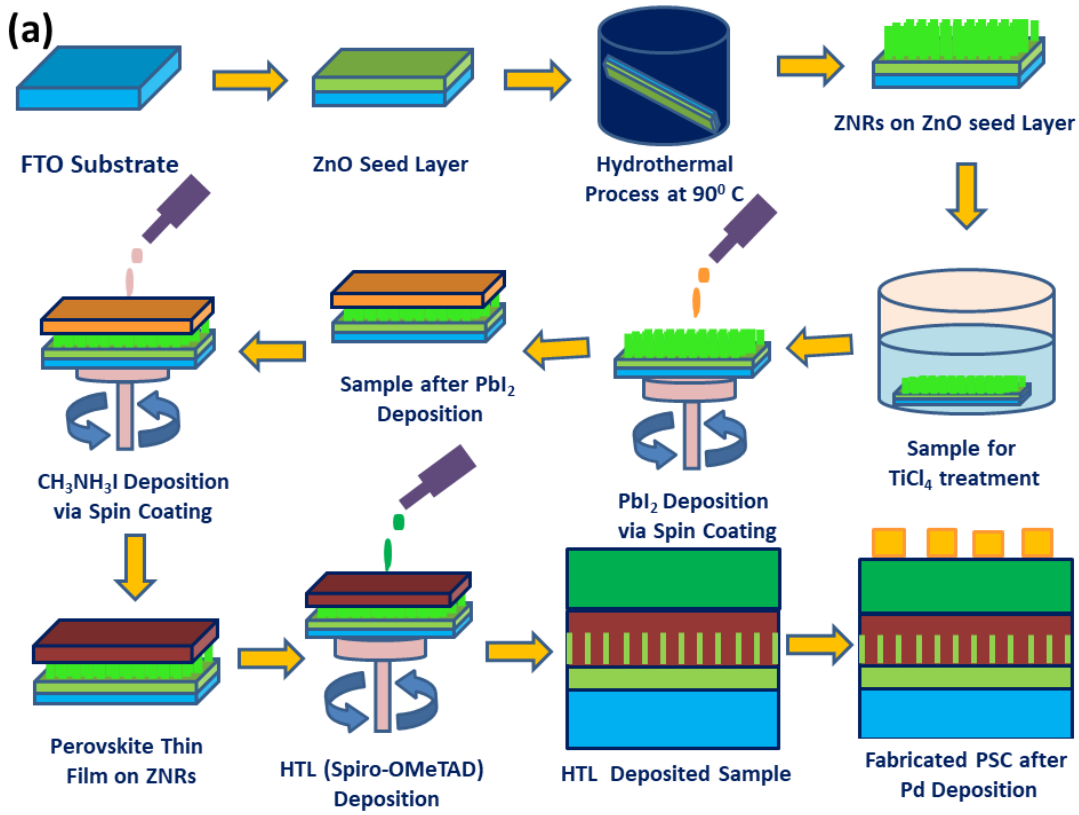

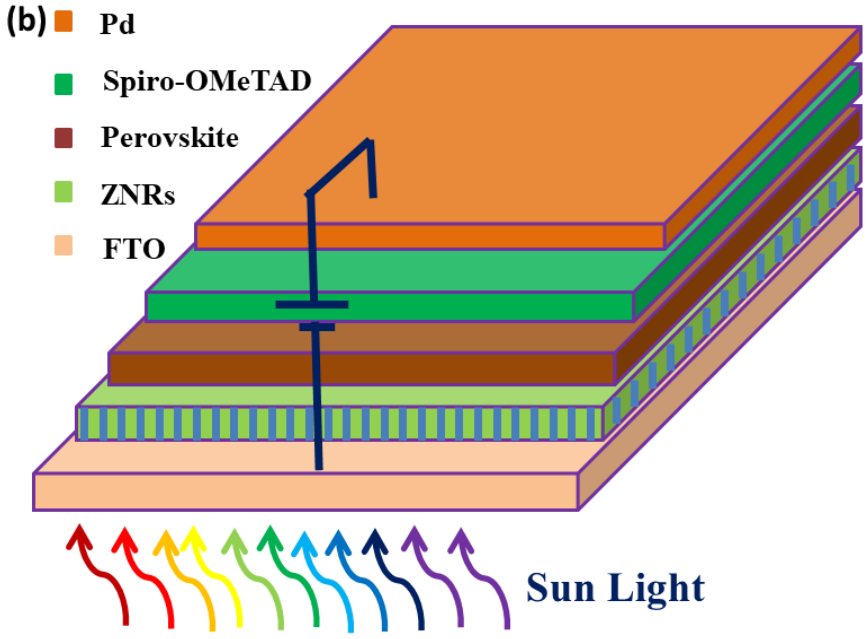

Figure 5.1: (a). Fabrication flowchart for the PSCs; (b) Complete device structure of the fabricated PSCs.

5.3 TCAD Simulation and Models

The carrier transportation in the proposed device structure is illustrated using a band diagram shown in Figure 5.2 (a). It can be observed that spiro-OMeTAD performs well as efficient HTL. The HTL efficiency improves further under doped condition. The fabricated device structure shown in Figure 5.2 has been considered for the simulation. The equivalent circuit [170] for the fabricated and simulated PSC is shown in Figure 5.2 (b). The current-voltage equation for the equivalent circuit is given as [173]:

$$J = J_0\{\exp[(q(v - JR_S))/\eta K_B T] - 1\} + \frac{V - JR_S}{R_{Sh}} - J_{ph} \quad (5.1)$$

Here, J and J_{ph} are the dark and photon current of the device. The J_0, q, η, K_B, R_S, R_{Sh} are the reverse saturation current density, carrier charge, ideality factor, Boltzmann constant, series resistance, and shunt resistance, respectively. The numerical simulation

has been performed using SetFos^{TM} (from Fluxim) TCAD simulation tool. The parameters used for the device simulation of the PSC are shown in Table 5.1.

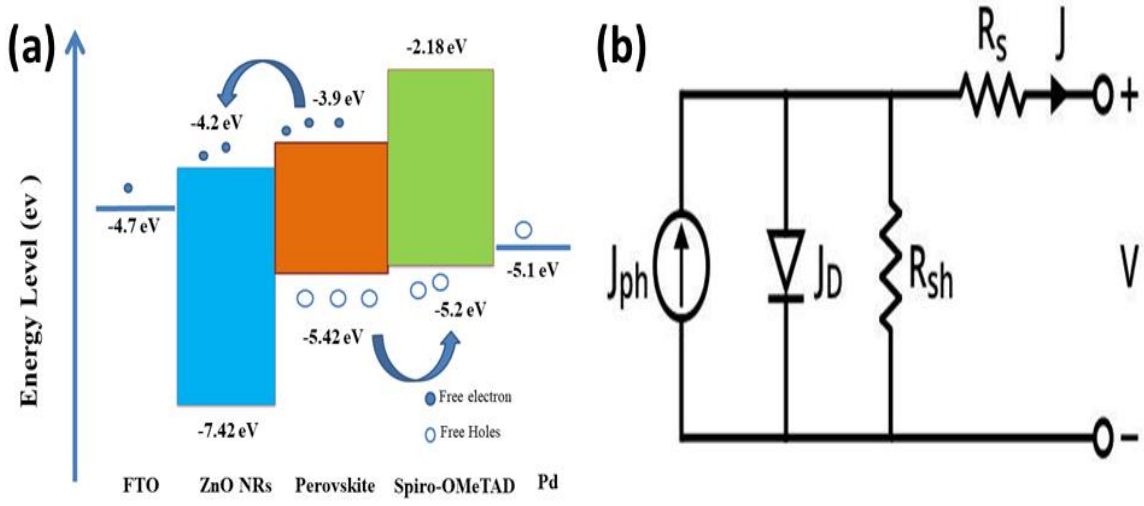

Figure 5.2: (a) Energy band diagram of perovskite solar cell and (b) Equivalent electrical circuit.

Table 5.1: Different parameters used in the simulation of PSCs.

Parameters	**ZNRs (ETL)** [126], [127], [174]	**Perovskite** [126], [127]	**Spiro-OMeTAD (HTL)** [122], [175], [176]	**Doped Spiro-OMeTAD (HTL)** [166], [169], [177]
Dielectric constant (ε_r)	9	10	3	3
Band gap (eV)	3.2	1.5	3	2.96
Electron affinity (χ)	3.9	3.85	2.45	2.45
Electron mobility ($cm^2/V\text{-}s$)	10	2.2	3.6×10^{-4}	1.6×10^{-3}
Hole mobility ($cm^2/V\text{-}s$)	2	2.2	3.6×10^{-4}	1.6×10^{-3}
VB effective DOSs (cm^{-3})	1×10^{18}	3×10^{18}	1.8×10^{19}	1.8×10^{19}
CB effective DOSs (cm^{-3})	1×10^{18}	1×10^{18}	2.2×10^{18}	2.2×10^{18}
Defect density (cm^{-3})	1×10^{14}	1×10^{15}	1×10^{13}	1×10^{13}
Acceptor concentration (cm^{-3})	0	1×10^{17}	1×10^{16}	1×10^{17}
Donor concentration (cm^{-3})	1×10^{19}	1×10^{17}	0	0

The simulation tool solves the following Poisson and continuity equation [178]:

$$\nabla^2\varphi = \frac{q}{\varepsilon}(n - p + N_A + N_D) \tag{5.2}$$

$$\nabla.J_n = q\frac{\partial n}{\partial t} + q.R \tag{5.3}$$

$$\nabla.J_p = -q\frac{\partial p}{\partial t} - q.R \tag{5.4}$$

Where ψ, N_A, and N_D are the electrostatic potential, acceptor, and donor concentration, respectively. The parameters R, J_n, and J_p are the rate of recombination, electrons, and holes current density, respectively. The drift-diffusion mechanism for electron and hole conduction is taken in the model. Here, drift phenomena is influenced by the internal electric field and the diffusion mechanism is happened due to concentration gradient. The equations used for drift-diffusion of electrons and holes conduction are:

$$J_n = q\mu_n nE + qD_n\nabla_n \tag{5.5}$$

$$J_p = q\mu_p nE + qD_p\nabla_p \tag{5.6}$$

Where μ_n, μ_p are the mobility of electron and hole. D_P and D_n are the diffusion coefficient for holes and diffusion coefficient for electrons.

5.4 Results and Discussion

In this section, first perovskite thin film and charge transport layers are characterized, and then solar cell characteristics are presented and discussed in detail.

5.4.1 Thin Film Characterization

The performance of the perovskite solar cell is improved by controlling the diameter and length of ZnO NRs. The ZnO NRs length is a function of the growth time, synthesis temperature, and the precursor concentration. The transmittance spectra of ZnO NRs treated with $TiCl_4$ is shown in Figure 5.3 (a). The relation between transmittance and absorbance is given as [116]:

$$A(\%) = -log_{10}T$$

The characteristic plot of the optical bandgap and the absorbance coefficient has been shown in Figure 5.3 (b). The relation between the optical band gap and the absorbance coefficient is given by equation [128]:

$$\alpha h\upsilon = A\left(h\upsilon - E_g\right)^m \tag{5.7}$$

Where, h, v, E_g, A, and m are Planck constant, frequency of light, optical band gap, absorbance, and material constant. And, $\alpha = 2.33\log\left(T/d\right)$ is the absorbance coefficient; where T is transmittance and d is film thickness. The estimated bandgap of the synthesized ZnO NRs is ~3.2 eV.

The surface roughness of ZNRs without treated and with $TiCl_4$ treated has been analyzed in dynamic mode. The obtained surface images are shown in Figure 5.4 (a) and (b). The surface roughness is expressed in terms of root-mean-square (rms) roughness values. The untreated ZnO NRs surface has rms roughness of 132 nm, whereas the $TiCl_4$ treated ZnO NRs surface has rms roughness of 110 nm. On the other hand, the deposited perovskite film has minimized the roughness on the surface. The

roughness of the perovskite deposited surface is shown in Figure 5.4 (c). The rms roughness is reduced to 80 nm on the perovskite deposited surface. The HRSEM image of ZnO QDs thin film (seed layer) on FTO is depicted in Figure 5.5 (a). The optimized ZnO NRs with an average length of ~450 nm and diameter of ~80 nm are synthesized as measured from the HRSEM image shown in Figure 5.5 (b).

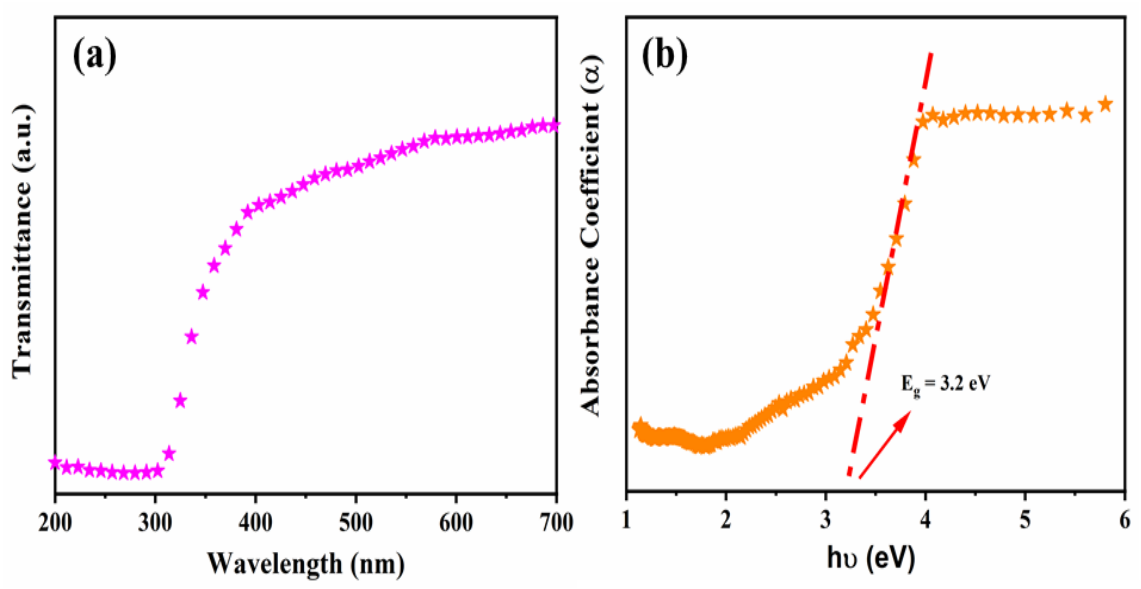

Figure 5.3: (a) Transmitance spectra of ZnO NRs and (b) Tauc plot for ZnO NRs.

The grain size and surface morphology of perovskite thin film deposited on ZnO NRs are depicted in Figure 5.5 (c). The thickness of perovskite film over ZnO NRs measured using cross-sectional HRSEM image is shown in Figure 5.5 (d).

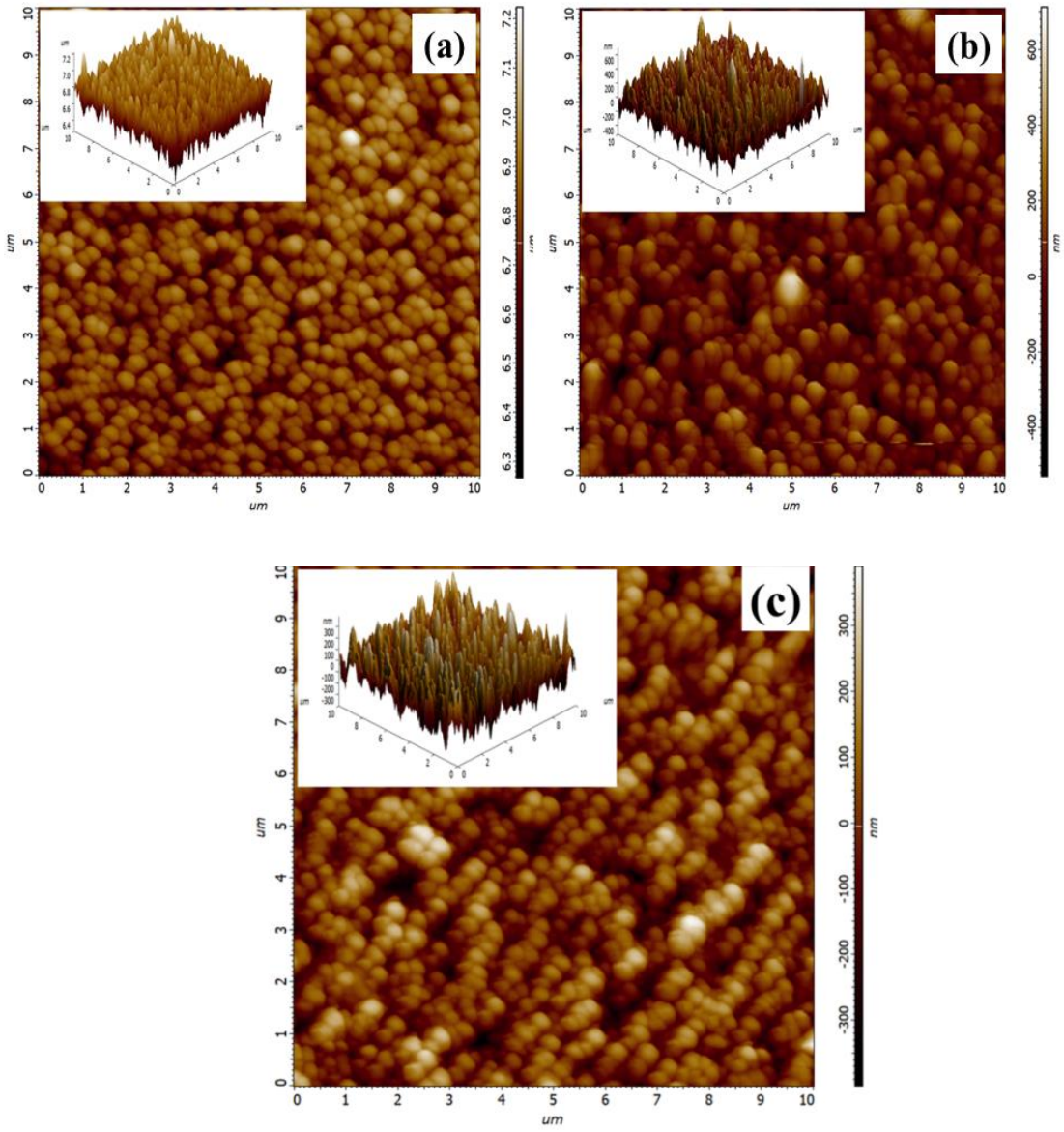

Figure 5.4: AFM image of (a) ZnO NRs without $TiCl_4$ treated, (b) ZnO NRs with $TiCl_4$ treatment, and (c) Perovskite layer on ZnO NRs

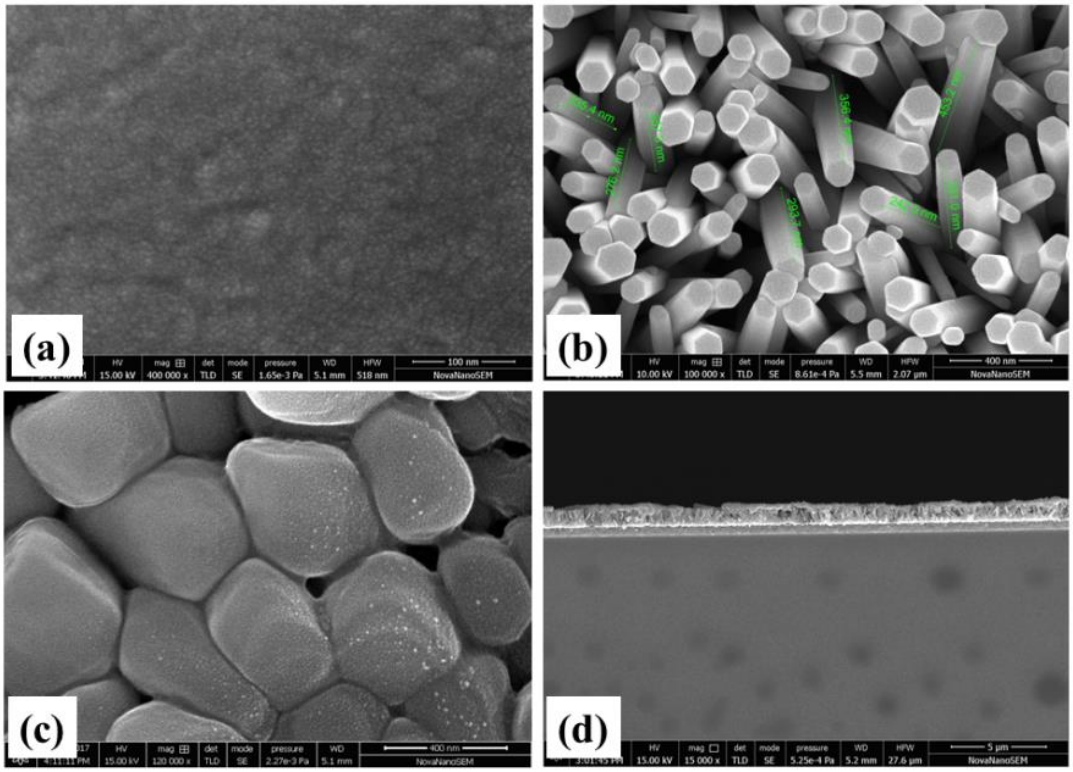

Figure 5.5: HRSEM image of (a) ZnO quantum dot, (b) Solvothermally synthesized ZnO NRs, (b) Perovskite thin film on ZnO NRs, and (d) Cross-sectional image of perovskite layer on ZnO NRs.

5.4.2 Solar Cell Characterization

The performance of PSC depends on the electrical and optical properties of HTM, ETM, and active layer materials. The film thickness for these layers has been optimized for the enhanced performance parameters of the PSCs. The ETL made of consecutive-grown ZnO NRs have some gap in the adjacent rods, and this void will lead to leakage current, which enhances the dark current. This also increases defect density, which reduces the performance of PSCs. Thus, the $TiCl_4$ treated ZnO NRs were used as ETL in the PSC structure. $TiCl_4$ treatment of ZnO NRs at an optimized temperature creates an ultrathin layer of TiO_2, which makes ZnO/TiO_2 core-cell structure [179]. The $TiCl_4$ treatment enhances the chemical stability of ZnO NRs and reduces the voids/defects. The two types of HTL (undoped spiro-OMeTAD and doped spiro-OMeTAD) based

PSCs have been characterized for their performance. It is observed that the doping reduces the impedance in the doped spiro-OMeTAD, as shown in the Nyquist plot in Figure 5.6 (a). This reduced impedance is due to increased carrier density in the doped spiro-OMeTAD, which results in improved PSC parameters. The impedance characteristics have been recorded over a frequency range of 1 kHz to 1 MHz under 100 mW/cm^2 (1.5 AM) illumination at a bias voltage of 900 mV. Based on impedance characteristics, the equivalent circuit for the PSCs having a series resistance as well as R_{rec} and C_{rec} in parallel combination along with R_{HTL} and C_{HTL} in parallel combination is shown in Figure 5.6 (b). Where series resistance (R_S) is related to contact resistance of individual layers and electrodes (Pd and FTO). The high-frequency region describes the behavior of hole diffusion in the HTL layer, which is denoted by the parallel combination of R_{HTL} and C_{HTL}. Whereas the lower frequency region shows the parallel combination of recombination resistance (R_{rec}) and capacitance (C_{rec}), which is related to the Fermi level of ETL [180]. The PSC with a doped HTL layer shows a smaller semicircle, which represents the better charge transportation compare to undoped HTL based PSCs [181]. Imaginary impedance (Z") vs. frequency graph has been shown in Figure 5.7 (a). This graph explains about the relaxation frequency, and the relaxation frequency is inversely proportional to relaxation time, i.e. ($f_{max} \alpha 1/\tau$). It can be seen from Figure 5.7 (a) that the relaxation frequency peak in doped HTL based PSC is shifted towards a higher frequency region in comparison to undoped HTL based PSCs, which implies a fast charge transportation rate in doped PSCs [181]. The relaxation time defines the charge transfer rate at the interface of the transport layer with the active layer. For the fast separation rate of the charge carrier, the relaxation time should be lower. Further, Figure 5.7 (b) shows the frequency-dependent real part of the

impedance, which corresponds to the R_{HTL} [180]. In Figure 5.7 (b), the PSC with doped spiro-OMeTAD shows a lower value of impedance as compared to the PSC with undoped spiro-OMeTAD, which confirms the transport layer exhibit the better interface in doped spiro-OMeTAD based PSC [182] that results in better performance.

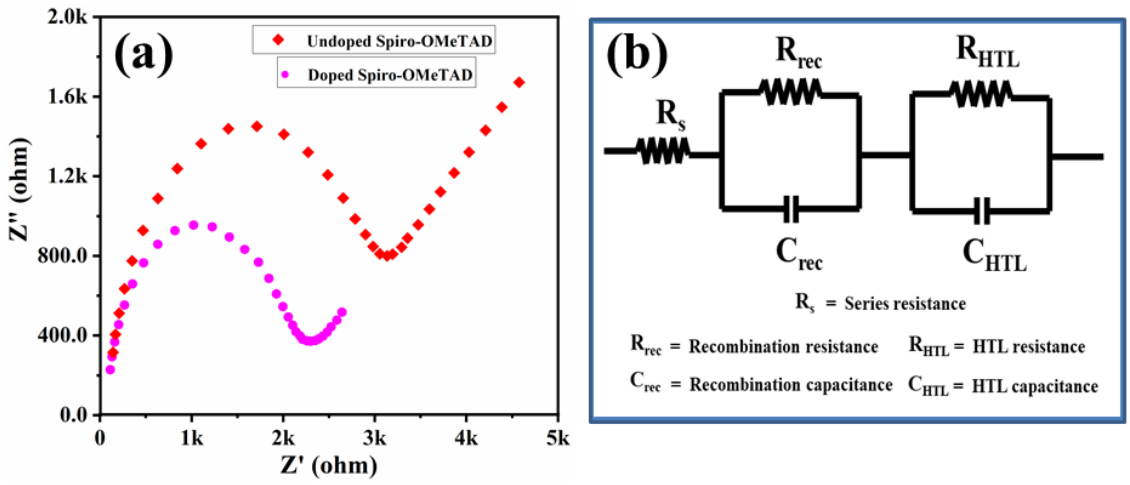

Figure 5.6: (a) Nyquist plot for fabricated PSC with undoped and doped HTL layer; (b) Equivalent circuit model employed using impedance characteristics.

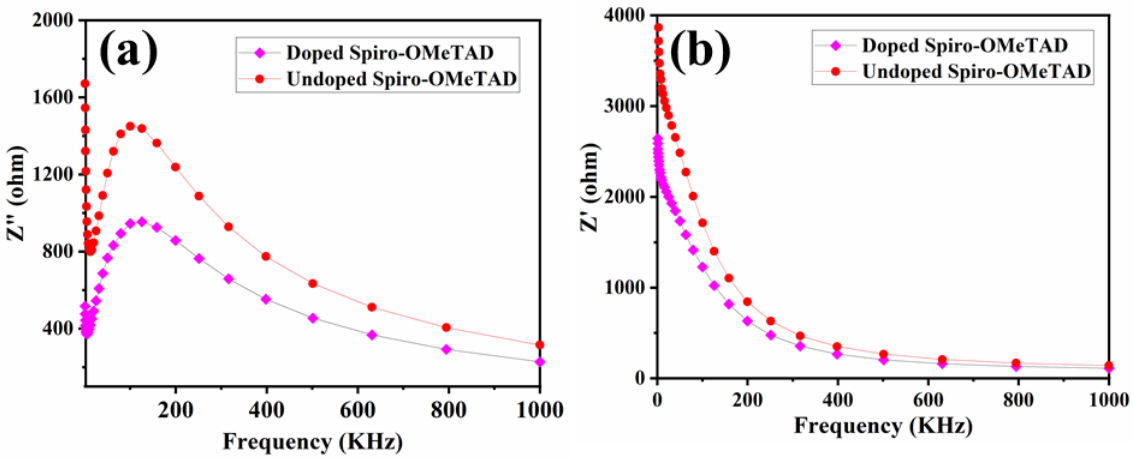

Figure 5.7: (a) Imaginary impedance vs. frequency plot, and (b) Real impedance vs. frequency plot of fabricated PSCs

The obtained electrical characteristics using the current-density vs. voltage (J-V) curve of the fabricated PSCs have been shown in Figure 5.8 (a) and 5.8 (b). Whereas the extracted parameters from the experimental finding (as shown in Table 5.1) are used in

the TCAD simulation to obtain the electrical characteristic of the solar cells as in Figure 5.8 (a) and (b). It is found that the simulated results are in good agreement with the experimental for both types of PSCs. The calculated solar parameters namely V_{OC}, J_{SC}, *FF*, and *PCE* from *J-V* characteristics of Figure 5.8 (a) are 0.98 V, 15.84 mA/cm^2, 61%, and 9.51 %, respectively for fabricated, whereas 1.001 V, 15.83 mA/cm^3, 0.60%, and 10.13%, respectively for simulated undoped spiro-OMeTAD based PSC. On the other hand, V_{OC}, J_{SC}, *FF*, and *PCE* calculated from *J-V* characteristics of Figure 5.8 (b) are found as 1.01 V, 18.53 mA/cm^2, 64%, and 10.18%, respectively for fabricated, whereas 1.001 V, 17.27 mA/cm^3, 0.66%, and 11.53%, respectively for simulated doped spiro-OMeTAD based PSC. The calculated solar parameters are compared in Table 5.2. The improved solar parameters in doped spiro-OMeTAD based PSC is due to increased charge carrier density and better band alignment.

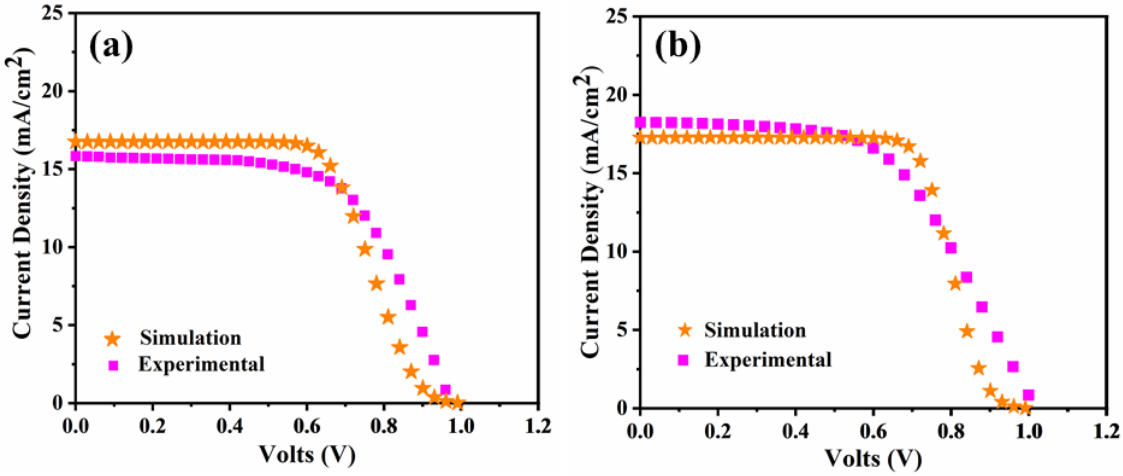

Figure 5.8: Current density vs. voltage curve for (a) Undoped spiro-OMeTAD and (b) Doped spiro-OMeTAD.

The external quantum efficiency (EQE) for both types of PSCs has been calculated from wavelength versus photocurrent characteristics. The monochromatic light of 350 nm to 800 nm is illuminated to the PSCs, and the corresponding photocurrent is

measured. The ratio of obtained photocurrent and optical power of incident light is defined as the responsivity (R) for the PSCs [183]. The EQE of the PSC is calculated using the responsivity characteristics [116]. The obtained EQE characteristics for both the PSCs have been shown in Figure 5.9 (a) and (b). It is observed that the EQE is slightly improved with doping and the simulated characteristics are in good agreement with the experimental.

Table 5.2: A comparison of fabricated and simulated PSC parameters.

	Simulation (Undoped spiro-OMeTAD)	Experimental (Undoped spiro-OMeTAD)	Simulation (Doped spiro-OMeTAD)	Experimental (Doped spiro-OMeTAD)
V_{OC} (V)	1.001	0.98 ± 0.1	1.001	1.01 ± 0.1
J_{SC} (mA/cm^3)	15.83	15.84 ± 0.35	17.27	18.53 ± 0.30
FF	0.60	0.61 ± 0.1	0.66	0.64 ± 0.1
PCE (%)	10.13	9.51 ± 0.2	11.53	10.18 ± 0.2

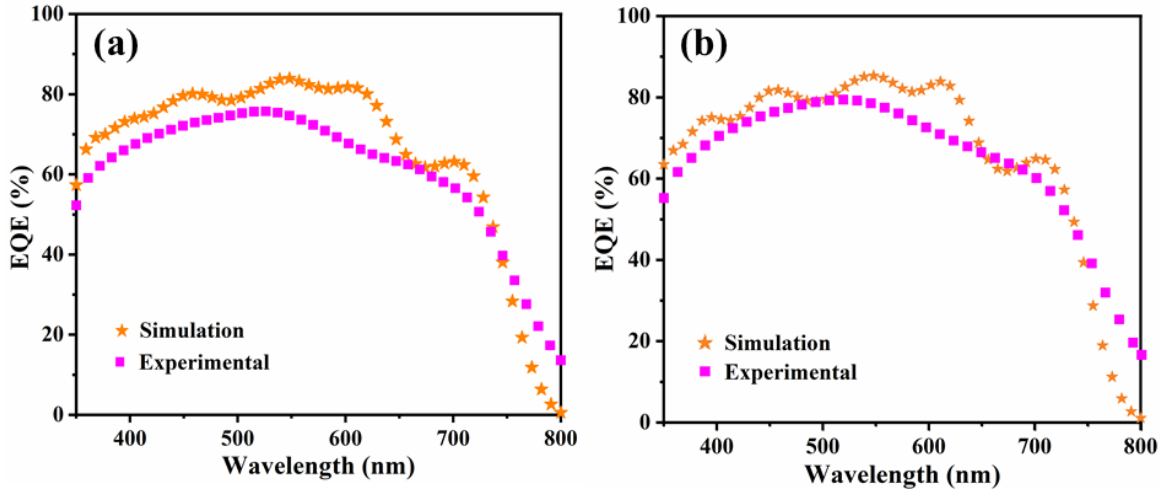

Figure 5.9: External quantum efficiency of (a) Undoped spiro-OMeTAD based PSC and (b) Doped spiro-OMeTAD based PSC.

5.5 Conclusion

In this chapter, the effect of both the undoped and doped spiro-OMeTAD HTL on the performance of a ZNRs ETL based FTO/ZNRs/Perovskite/Spiro-OMeTAD/Pd solar cell structure has been studied. The p-type dopant TBP and LiTFSI in the spiro-OMeTAD are used to improve the performance by enhancing the hole carrier density in the HTL. For undoped HTL, the proposed PSC gives an optimized *PCE* value of 10.18 % with V_{OC} of 1.01 V, J_{SC} of 18.57 mA/cm^2, and fill factor (*FF*) of 64% under ambient-air environment. However, improved performance with *PCE* of 11.53%, V_{OC} of 1.001 V, J_{SC} of 17.27 mA/cm^2, and *FF* of 0.66 are obtained for the doped spiro-OMeTAD HTL based PSC. The results have also been compared with the commercially available Set-Fos^{TM} TCAD tool for showing the reliability of the measured data. The reasonably good matching is observed between the experimental results and TCAD simulation data.